

Strongly (001) Oriented Bimorph PZT Film on Metal Foils Grown by *rf*-Sputtering for Wrist-Worn Piezoelectric Energy Harvesters

Hong Goo Yeo, Tiancheng Xue, Shad Roundy, Xiaokun Ma, Christopher Rahn, and Susan Trolier-McKinstry*

For piezoelectric energy harvesters, a large volume of piezoelectric material with a high figure of merit is essential to obtain a higher power density. The work describes the growth of highly (001) oriented sputtered lead zirconate titanate (PZT) films ($f \approx 0.99$) exceeding $4 \mu\text{m}$ in thickness on both sides of an Ni foil to produce a bimorph structure. These films are incorporated in novel wrist-worn energy harvesters ($<16 \text{ cm}^2$) in which piezoelectric beams are plucked magnetically using an eccentric rotor with embedded magnets to implement frequency up-conversion. The resulting devices successfully convert low-frequency vibration sources (i.e., from walking, rotating the wrist, and jogging) to higher frequency vibrations of the PZT beams (100–200 Hz). Measured at resonance, six beams producing an output of 1.2 mW is achieved at 0.15 G acceleration. For magnetic plucking of a wrist-worn non-resonant device, 40–50 μW is produced during mild activity.

1. Introduction

Energy harvesting has recently attracted attention for wireless sensor nodes and wearable electronics in combination with low power consumption electronic devices. Thus, considerable research has been directed toward self-powering devices

to eliminate the need to change or manually recharge batteries. Mechanical energy harvesters using piezoelectric materials such as lead zirconate titanate ($\text{Pb}(\text{Zr}_x\text{Ti}_{1-x})\text{O}_3$, or PZT) are promising for energy scavenging from environmental sources, including human motion.^[1] Two main strategies to enhance the performance of the harvester are commonly considered: exploitation of advanced mechanical designs and improvement of the piezoelectric material itself.

For a cyclically strained piezoelectric energy harvester (PEH), the root-mean-square (RMS) power output is given as: $P_{\text{rms}} = \frac{\omega}{4} \left(\frac{e_{31}^2}{\epsilon_0 \epsilon_{33}^T} \right) (At) S_i^2$,^[2] where the materials figure of merit (FoM) is $\frac{e_{31}^2}{\epsilon_0 \epsilon_{33}^T}$ (e_{31}

is the in-plane piezoelectric strain coefficient, and ϵ_{33}^T is the relative permittivity). The volume of the piezoelectric is its area \times thickness = At , and S_i is the strain magnitude. Thus, essential to achieving high power density ($\mu\text{W G}^{-2} \text{ cm}^{-2}$) in the 31 mode is preparation of thick films with high energy harvesting figures of merit that are capable of sustaining high strains without microcracking.^[3] The FoM can be maximized by preparation of strongly (001) textured PZT films.

Although there are previous reports on highly (001) oriented, dense PZT films, most of these describe films with 0.5–4 μm thickness on Si ,^[4–10] where the figure of merit for energy harvesting is low. In this work, a high-temperature sputtering approach was adopted to grow thick PZT films on both sides of Ni foils. The Ni foil imposes a compressive stress on the piezoelectric films due to the mismatch in thermal expansion coefficients; this compressive stress is essential to orienting the spontaneous polarization out-of-plane, which maximizes the figure of merit.

To demonstrate the efficacy of the thick PZT films prepared by high-temperature sputtering for a wearable PEH, the resulting films were incorporated into a novel wrist-worn structure. Conventional resonant harvester designs do not efficiently extract electrical energy from human motion due to nonperiodic excitation with components over a broad range of frequencies and various directions of acceleration.^[11–13] Recently, many reports have proposed alternative design strategies to overcome these limitations and challenges.^[14–19] One strategy for ultralow-frequency vibration is to convert the low-frequency excitation caused by the mechanical source to a

Dr. H. G. Yeo,^[†]

Department of Materials Science and Engineering and Materials Research Institute University Park, PA 16802, USA

Dr. T. Xue, Prof. S. Roundy


Department of Mechanical Engineering University of Utah 1495 E 100 S, Salt Lake City, UT, USA

Dr. X. Ma, Prof. C. Rahn

Department of Mechanical and Nuclear Engineering The Pennsylvania State University University Park, PA 16802, USA

Prof. S. Trolier-McKinstry

Materials Science and Engineering Department and Materials Research Institute The Pennsylvania State University University Park, PA 16802, USA E-mail: stmckinstry@psu.edu

 The ORCID identification number(s) for the author(s) of this article can be found under <https://doi.org/10.1002/adfm.201801327>.

^[†]Present address: DGIST-ETH Microrobot Research Center, Daegu-Gyeongbuk Institute of Science and Technology (DGIST), Daegu 42988, South Korea

DOI: 10.1002/adfm.201801327

higher frequency vibration of the piezoelectric material via repulsive/attractive magnetic coupling or mechanical plucking (e.g., frequency up-conversion designs).^[14–17] For example, Pilatsch et al. proposed a frequency up-conversion design with a permanent magnet and a 130 μm thick piezoelectric layer on a 110 μm thick carbon fiber center shim. The rotational harvester utilized the rotation of an eccentric proof mass to magnetically pluck the piezoelectric beam.^[15] In that energy harvester, the PZT beam had to be long (19.5 mm) due to the use of a stiff PZT bulk ceramic; the resulting structure had poor free oscillation and produced low output power.^[15]

This clearly demonstrates that many PEHs, especially those constructed using bulk piezoelectrics, are too stiff to be readily excited by modest accelerations at low frequencies, as is characteristic of human motion. In contrast, piezoelectric layers on more flexible substrates offer considerably more design room to accommodate available mechanical excitations.^[20] For example, a ZnO piezoelectric generator on a flexible Al foil was shown to enable energy harvesting from gentle wind.^[21] Given the modest energy harvesting figure of merit of ZnO films, PZT films on flexible metal foils provide a promising platform for frequency up-converting harvesters in wearable devices.

In this work, wrist-worn PEHs based on a frequency up-conversion mechanism using multiple magnetically plucked flexible piezoelectric beams were designed and fabricated. The magnetic plucking configuration is schematically shown in **Figure 1a**. The piezoelectric beam is deflected by the repulsive force between a fixed magnet (on the end of the beam) and a moving magnet (embedded in an eccentric rotor which couples

to wrist motion). The highly (001) oriented bimorph PZT thick films on Ni foils survive large strains, and enable high power outputs from wrist-worn devices. Furthermore, because the frequency up-conversion is achieved without the use of gears (typical for electromagnetic generators) or mechanical contact, there is very little mechanical loss. The result is that this plucked piezoelectric harvester is capable of generating usable power output (i.e., 10's of μW more) under very light excitations.

2. Results and Discussion

High-temperature *rf*-magnetron sputtering was selected for the growth of thick PZT films with high density and the desired (001) orientation based on the work of Fujii et al. who reported preparation of ≈ 4 μm thick Nb-doped PZT films on a stainless steel substrate.^[5] Sputtering also allows sequential deposition of oriented PZT films on both sides of a substrate to produce a bimorph. This both increases the volume of piezoelectric, and allows the output voltage of a given film in a bimorph structure to be approximately doubled relative to that of a unimorph without increasing the total area of the device. However, challenges are encountered in the growth of a phase-pure PZT film at elevated temperatures due to the volatility and propensity for resputtering of PbO.^[6,7] Consequently, the amount of excess Pb in the PZT target, the oxygen and Ar pressure, and the substrate temperature were optimized, as described elsewhere.^[8–10]

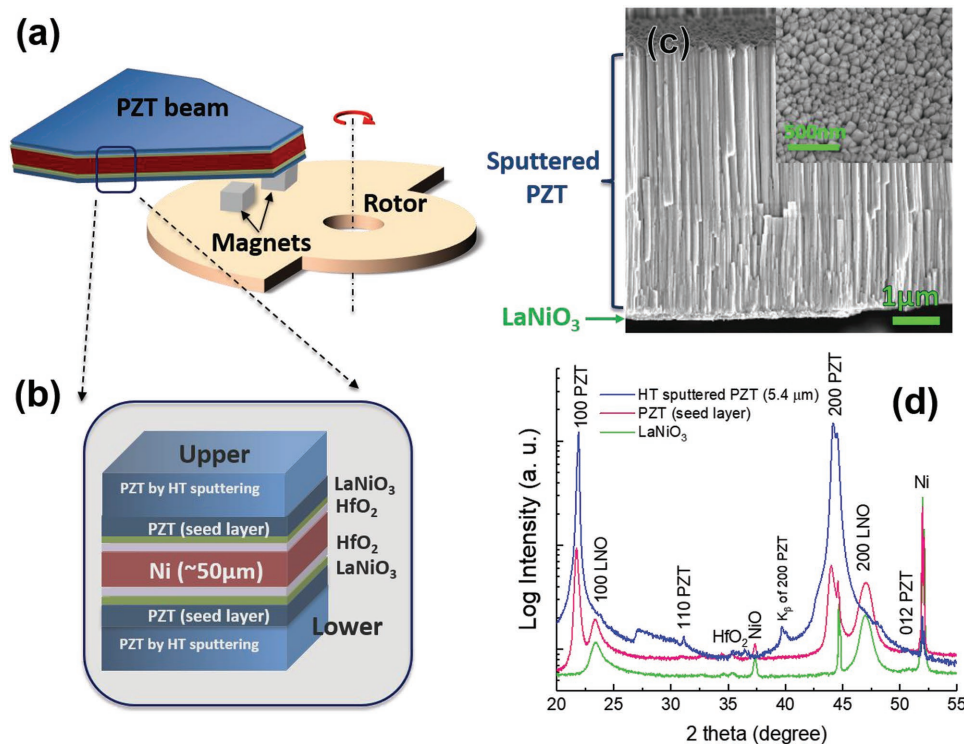


Figure 1. a) Functional principle of the rotational harvester with bimorph PZT beam. b) Schematic cross-section of as-grown PZT, PZT seed layer, LaNiO₃ template, and HfO₂ passivated Ni foil bimorph. c) Cross-section and surface (inset picture) FESEM images of 5.4 μm layers of PZT sputtered with in situ crystallization. d) XRD $\theta - 2\theta$ scan of high-temperature sputtered PZT, seed layer (PZT), and LaNiO₃.

2.1. Characterization of Bimorph PZT Films on Ni Foil

For in situ crystallization during sputtering, excessive evaporation or resputtering of Pb from the growing film leads to formation of Pb-deficient pyrochlore phases.^[22] Thus, it is important to control the Pb content to achieve the desired stoichiometry. In practice, this can be done via the optimization of parameters such as the amount of Pb excess in the target and the chamber pressure. Based on a series of experiments, an optimized deposition procedure for the Lesker sputter tool was developed (see Figure S3, Supporting Information). As has been reported elsewhere, the Pb content in the growing film decreased as the substrate temperature increased above ≈ 500 °C during deposition.^[23–27] Comparatively low deposition temperatures were employed (< 650 °C) to reduce thermal stresses so that thick, uncracked films could be grown. Stringent control of the nucleation and growth process^[28,29] was achieved using a PZT seeding layer. Comparing high-temperature sputtering of PZT films on Pt/Si substrates with and without seed layers (in Figure S8b,c, Supporting Information), it is clear that the seed layer enables growth of well-crystallized films without second phases.^[28,30] Thus, a (001) oriented PZT seed layer was used to facilitate nucleation of the perovskite structure with the desired orientation to obtain a high figure of merit for the PEH.^[8,31–33]

PZT films were sputtered on a (001) PZT seed layer/(100) $\text{LaNiO}_3/\text{HfO}_2/\text{Ni}$. The Ni foils were 50 μm in thickness. Details on the substrate processing up to the LaNiO_3 layer are provided elsewhere.^[32] The crystallized PZT seed layer (≈ 70 nm thick) was prepared by chemical solution deposition (CSD) with 15 wt% of 10% Pb excess PZT (52/48) Mitsubishi Materials solution. As shown in Figure 1d, PZT layers deposited using the optimized deposition conditions on the seed layer show well oriented (001) perovskite peaks, without any indication of intermediate pyrochlore phase. Figure S1 (Supporting Information) shows the surface microstructure of the dense PZT layer; it has a similar grain size and shape as was observed in previous work.^[32] A larger scale optical image shows reasonable thickness uniformity across the foil. Thus, for the deposition conditions described in Table S1 (Supporting Information), (001) oriented PZT (52/48) thin films can be grown on (001) oriented PZT seed layers using in situ crystallization by sputtering at a substrate temperature > 550 °C.

The crystallinity of each layer in Figure 2b was assessed by X-ray diffraction (XRD) patterns taken after each successive PZT layer was grown. The XRD exhibits strongly (001) oriented perovskite peaks for each as-deposited PZT layer as shown in Figure S2 (Supporting Information). Although the first layer shows a small amount of intermediate pyrochlore phase (marked with a star), it was completely converted to the perovskite phase by postdeposition annealing in an rapid

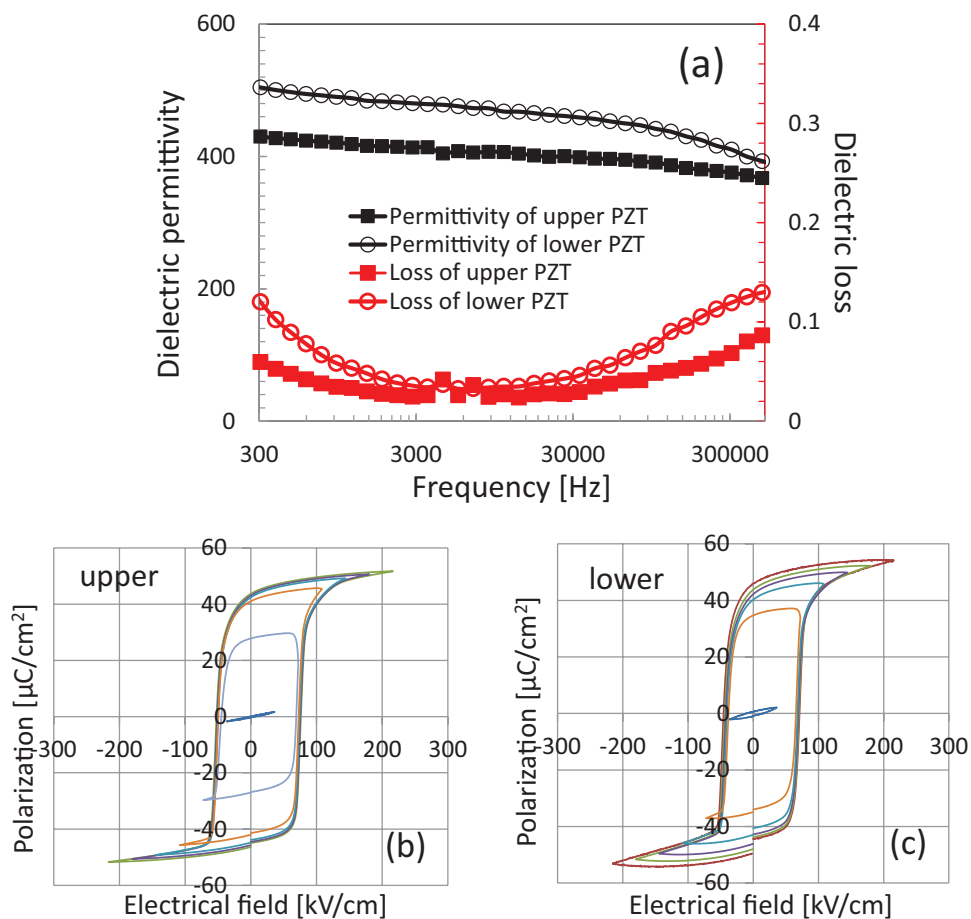


Figure 2. Electrical property measurements for both PZT layers on Ni foil grown by high-temperature sputtering. a) Dielectric constant and loss tangent of upper and lower PZT layer. Polarization–electric field hysteresis of b) upper and c) lower PZT layer.

thermal annealer (RTA) for 1 min at 650 °C. The deposition of the 5.4 μm thick PZT layer was achieved in three 1.8 μm steps.

Improved crystallization was observed as the substrate temperature was increased for the growth of each additional PZT layer. By following the same procedure, the reverse (back) side of the Ni foils was also deposited alternately three times with 1.8 μm thick sputtered PZT layers to reach a 5.4 μm thick PZT film. 5.4 μm thick bimorph PZT layers were achieved by high-temperature sputtering with high levels of (001) orientation, as represented by a Lotgering factor ($f_{(001)}$) of 0.99. This represents a significant improvement in both texture and thickness relative to our previous work with the 3 μm thick bimorph PZT films obtained by room *r*f-sputtering with postannealing ($f_{(001)}$) of upper and lower PZT layer is 0.75 and 0.74, respectively, as shown in Table S2, Supporting Information). A columnar structure with 50 to 90 nm of pyramid-shaped dense grains were observed in the surface microstructure and cross section images in Figure 1c. High-temperature sputtered PZT films show no significant pores unlike the previous work for sputtered PZT films with postannealing crystallization which exhibit porosity as a result of PbO volatilization during the crystallization.^[33–36] The higher density increases ϵ_{ij} ^[4] These pyramidal columnar grains and grooved grain boundaries produce a rough surface topography. The rough surface could cause electric field concentration, especially at grooved grain boundaries, which can lead to electrical breakdown.^[37] To reduce the surface roughness, one CSD PZT capping layer was grown on both sides of the as-deposited sputtered PZT layers.

The dielectric constant and loss of the upper and lower PZT films were measured by an inductance - capacitance - resistance (LCR) meter at 30 mV AC voltage signal from 300 Hz to 300 kHz. Dielectric constants (ϵ_r) of 410 and 470 with low losses of 0.03 and 0.035 were observed for the upper and lower PZT layers, respectively, at 10 kHz, as shown in Figure 2a. The polarization–electric field (*P*–*E*) hysteresis loops of both PZT layers have square shapes with large remanent polarizations (Figure 2b,c). The low dielectric constants and large remanent polarizations are characteristic of (001) oriented PZT films with large *c*-domain populations.^[31,32] Such films show significant promise for enhancement of the FoM of the PEH.^[8]

2.2. Characterization of Wrist-Worn Piezoelectric Energy Harvesters

A wrist-worn piezoelectric harvester was designed with six trapezoidal cantilever beams with attached permanent

magnets (Figure 3a); each beam is excited based on out-of-plane magnetic plucking as shown schematically in Figure S10 (Supporting Information). 1 mm tip displacement in the out-of-plane direction produces an average strain of ≈0.03% on the surface. This can be induced by 0.05 N of transverse force using 2 mm³ size of NdFeB magnets as predicted by finite element analysis of one trapezoidal beam.

The trapezoidal beam improves the strain distribution applied to the piezoelectric, relative to a rectangular cantilever beam.^[38] This design also utilized large area top electrodes of 1.54 cm² to maximize efficiency. The interaction between the magnet on the piezoelectric beam and the magnet in the rotor creates an out-of-plane force that plucks the beam and an in-plane force that tends to slow down the rotor and can even cause it to stop (i.e., it creates a detent or cogging torque). In order to overcome the detent torque, a larger rotor inertia is desirable. Most of the rotor was machined from brass with a density of 8.7 grams per cubic centimeter (g/cc). Heavier tungsten weights (density = 19.3 g/cc) were incorporated into the rotor to increase the inertia.

Before assembly, each trapezoidal PZT beam was characterized using a shaker table excited at the beam resonance frequency to validate its functionality. Figure 4a shows a trapezoidal beam (in the green box) placed on the shaker vertically and held with a customized plastic clamp. Without a proof mass (the neodymium magnet), the resonance frequency of the beams was 250 Hz. In Figure 4b, it is observed that the open circuit voltage (blue line) is up to 6.6 V_{pk-pk} for the PZT layers in a series connection when the beam was shaken at 0.15 G [$G = 9.8 \text{ ms}^{-2}$] excitation (yellow line).

To measure the maximum output, the external load resistance was varied (as in ref. [32]) at the resonance frequency (250 Hz) and an excitation level of 0.15 G. Figure 4c exhibits the maximum output power as a function of the external load resistance (for a parallel connection of the load). A maximum generated power ($P_{\text{max}} = V_{\text{max}}^2/R$) of 201 μW with maximum voltage ($V_{\text{max}} = V_{\text{pk-pk}}/2$) of 1.85 V was obtained at a load resistance of 17 kΩ for series connection. For six beams, this enables 1.2 mW for the maximum generated power.

Table 1 shows a comparison of the trapezoidal bimorph and a cantilever unimorph PZT beam, with their active area, resonance frequency, generated power, and area power density. The power density of the trapezoidal bimorph PZT (5.4 μm thick) beam is three time higher than that of 3 μm thick PZT layer sputtered on the rectangular cantilever. The enhancement

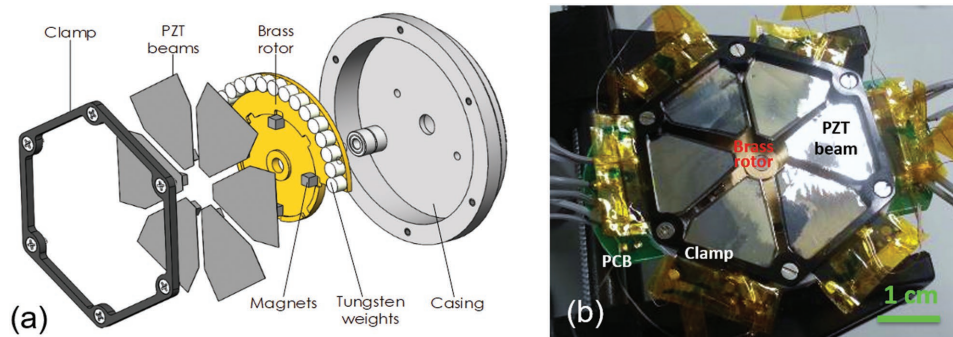


Figure 3. a) Illustration of PZT beams, rotor, and magnets for the flower petal wrist harvester. b) Image of a completed device.

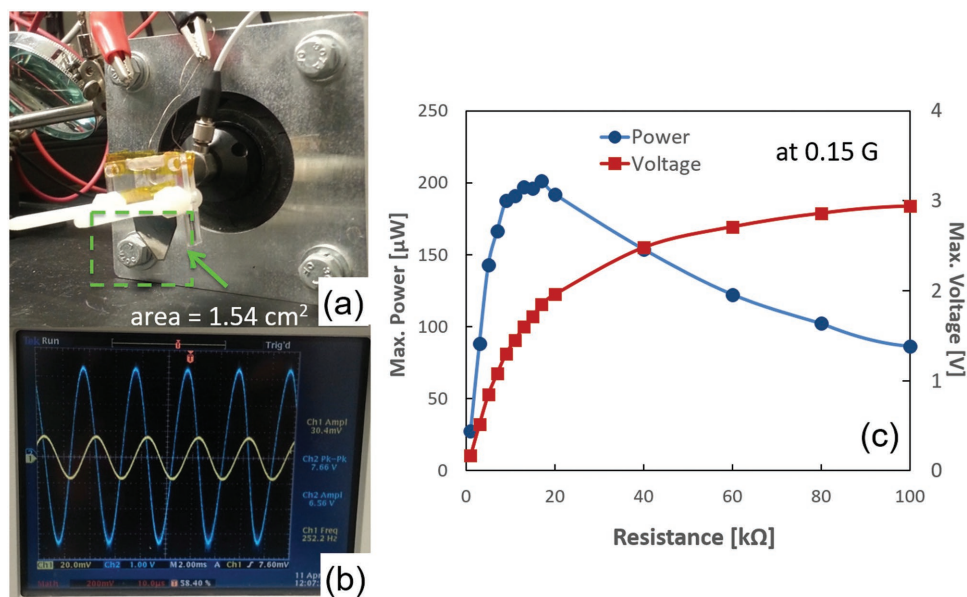


Figure 4. a) Experimental setup to measure the response as a function of vibration amplitude at the resonance frequency for one trapezoidal bimorph PZT beam (green box) for the wrist-worn harvester. b) V_{OC} (Ch2; blue) and acceleration waveform (Ch1; yellow) read out by an oscilloscope (TDS3054C, Tektronix). c) Relationship between maximum power and the external load resistance for the bimorph trapezoidal PZT beam.

of power density is likely to be due to a combination of the increase of PZT volume and improvement in the strain distribution using the trapezoidal beam shape.^[38]

Figure 5a depicts the magnet configuration for the wrist-worn harvester. There is a 1 mm gap and 1.3 mm offset between magnets. This should enable 1 mm of tip displacement and an average strain on surface 2.82×10^{-4} . 2 mm³ neodymium magnets were attached on the end of 5.4 µm thick bimorph PZT film on Ni and rotor based on the simulation results for the wrist-worn harvester.

Before assembling all of the trapezoidal beams, a single beam with an attached permanent magnet, as seen in the inset in Figure 5b, was tested to understand the static behavior and to compare the results to simulation. This allowed the mechanics to be understood without complications introduced by magnetic coupling between adjacent beams. In order to determine the resonance frequency, a beam was manually deflected, released, and allowed to ring down (in Figure 5b). The measured resonance frequency was around 130 Hz, which is very close to the 129.2 Hz in the simulation for a tapered cantilever beam with tip magnet.

In the actual prototype, the beam is actuated by a repulsive magnetic force, which creates a magnetic stiffening force that alters the cantilever characteristics. Figure 5c reveals the beam

tip displacement and voltage output across an 18 kΩ resistor in the presence of the stiffening force while the beam was displaced manually and released. The resonance frequency, under the effect of this stiffening force, was measured at 180 Hz. The mechanical quality factor ($Q = 1/(2\zeta)$, where ζ is the damping ratio of the beam) was determined to be 28 using the standard logarithmic decrement method.

When all beams are assembled in the prototype, the proximity of the tip magnets on adjacent beams creates an undesirable magnetic interaction between beams, which results in resting curvature in some beams. This phenomenon can be mitigated or even eliminated by increasing the gap between adjacent magnets to weaken the coupling.

The assembled wrist-worn device with six trapezoidal PZT beams was characterized using a device designed to simulate a pseudo wrist-worn situation. In the pseudo walking test, the PZT beams were plucked by the swinging motion (red arrow) of an aluminum arm that was controlled by a stepper motor (Figure 6a) that provided various swing angles and speeds in a sine wave.

Figure 6d shows the output voltage and power versus time of one unimorph beam produced by a human subject jogging in place with the device located on the wrist. The average, or RMS power produced by this unimorph beam is 13.05 µW. Based on

Table 1. Comparison of performance of two piezoelectric energy harvesters: a rectangular cantilever unimorph beam with 3 µm of PZT and a bimorph trapezoidal beam with 5.4 µm thick bimorph PZT.

Reference	Active material, mode	Device area [cm ²]	Acceleration [G]	Frequency [Hz]	Power _{rms} [µW]	Power density [µW cm ⁻² G ⁻²]
PSU cant.	3 µm PZT film by sputtering on Ni d ₃₁	0.385	0.15	72	9	1036
PSU Trapezoid	5.4 µm bimorph PZT, d ₃₁	1.54	0.15	250	100	2886

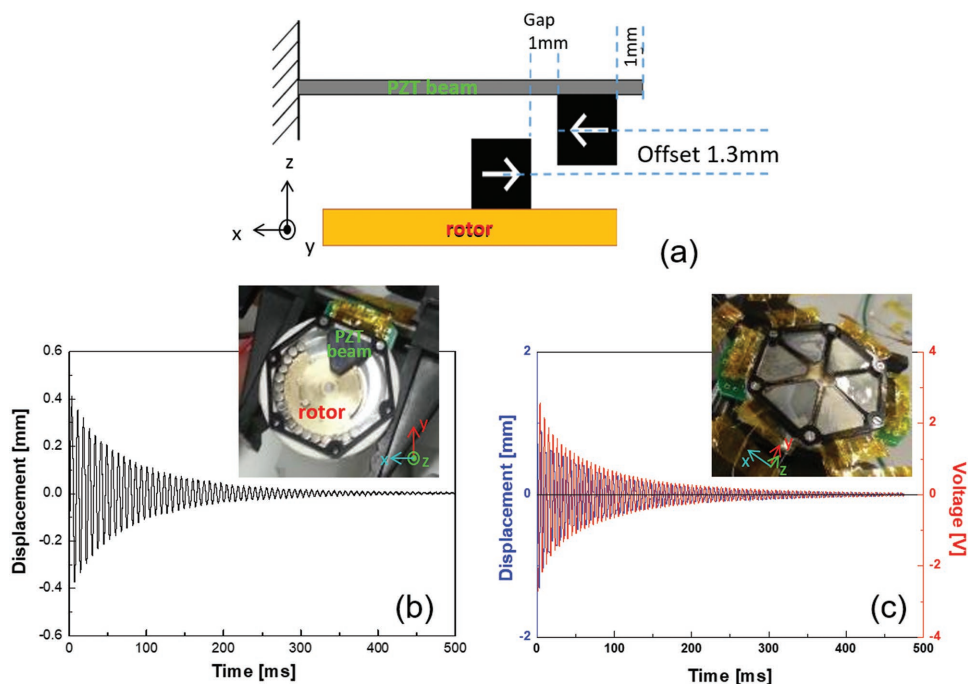


Figure 5. a) Configuration of magnets. b) Tip displacement measured from bend and let go input (inset: photograph of one trapezoidal beam assembled with one pair of magnets placed at the end of beam and on rotor). c) Displacement (blue line) and produced voltage (red line) resulting from manually bending the tip and letting go (inset: photograph of assembled six trapezoidal beams).

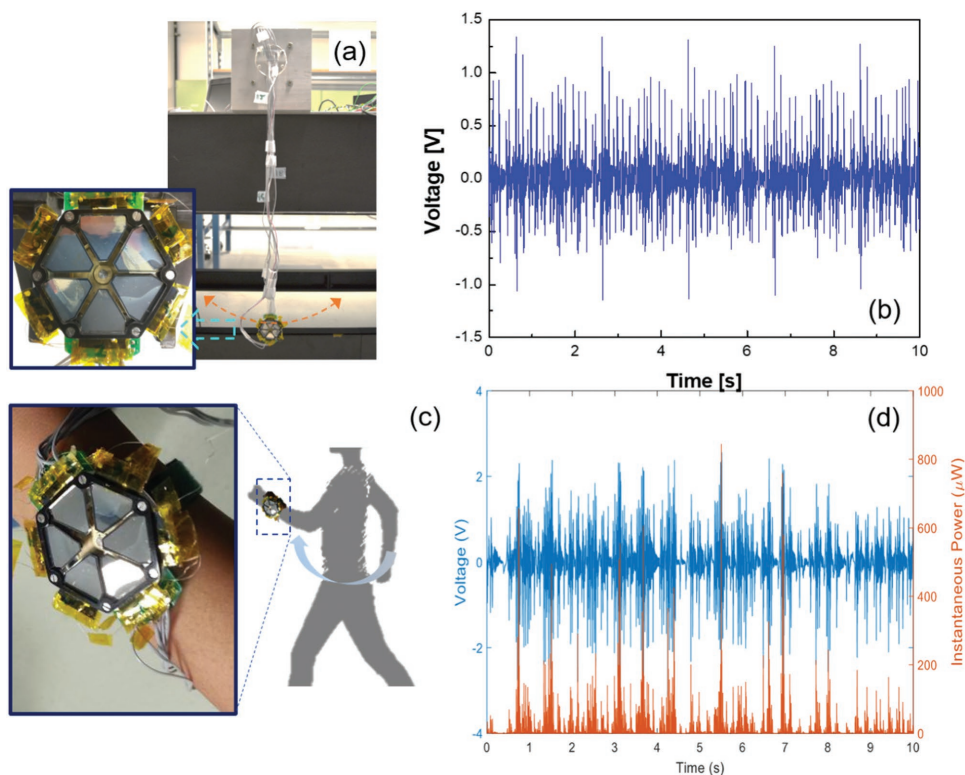


Figure 6. a) Experimental setup for swing arm test attached with wrist-worn device on the arm. b) Output voltage from one unimorph beam across 18 k Ω resistor during the pseudo walking on bench (angular rotation speed $T = 1$ s from -30 to $+30$ degree). RMS power output for this beam is 3.5 μ W. c) Images of device being worn on a wrist. d) Output from one unimorph beam across 27 k Ω resistor during jogging in place on wrist. RMS power output for this beam is 13.05 μ W.

Table 2. Summary of performance of wrist-worn device.

Input		Total RMS power from 6 beams [μW]	Total RMS power [μW] (best unimorph $\times 12$)
Pseudo walking on bench $30\sin\frac{2\pi t}{T}$	$T = 4 \text{ s}$	0.9	3
	$T = 2 \text{ s}$	1.7	6.4
	$T = 1 \text{ s}$	10.3	41.8
	$T = 0.5 \text{ s}$	19.5	48.2
On wrist	Jogging in place	38.3	156.6
	Rotating the wrist from -90 to $+90$ (arm hold horizontal)	25.1	91.4
Shaking in hand	Rotor in continuous rotation	37.8	158.8

the output power from the best performing unimorph beam in Figure 6d, the optimal RMS power (calculated by multiplying the power from the best electrode by 12) of $156.6 \mu\text{W}$ is predicted under a jogging-in-place excitation. The amount of power is similar to the power produced simply by holding the prototype in hand and shaking continuously.

Table 2 shows the RMS output power from the swing arm test for different sinusoidal swing motions (measured across $33 \text{ k}\Omega/18 \text{ k}\Omega$ resistor for bimorphs and unimorphs, respectively) and on body (across $56 \text{ k}\Omega/27 \text{ k}\Omega$ for bimorph and unimorph) test. The optimal load resistance can be approximately predicted by the model (load resistance $\approx 1/(2\pi \times \text{natural frequency} \times \text{capacitance})$). Since it is not a standard base excitation, the optimal load may depend on the excitation intensity. The experimental output power of the wrist-worn device increased with increasing angular rotation speed from -30° to $+30^\circ$ using the swing arm bench (Table 2). However, all six beams in the full harvester assembly did not perform equally well. It is believed that the other beams were mechanically damaged during handling and assembly. Moreover, strong magnetic coupling between beams required alternate beams to be bent up to reduce the magnetic repulsive force. Good power output was obtained from one unimorph beam during on body tests such as jogging and rotating the wrist without vertical movement. One of the beams in a fully assembled wrist-worn device was able to instantaneously flash a light-emitting diode when shaken by hand, as shown in Video S1 (Supporting Information). Furthermore, the device does not produce any adverse feeling to the wearer during normal daily activities.

For comparison, the RMS power output of a commercial self-powered watch generator (Kintron MGS^[39]) on the same aluminum swing arm was measured. The commercial generator has a “deadband” angle of about 10 degrees meaning that if the rotor displaces by less than ± 10 degrees no power is generated. Furthermore, the commercial generator has a higher level of mechanical loss (i.e., damping) due, in part, to a gearing system used to up-convert the frequency of the electrical signal. The result of these two effects is that at very light excitations no power, or extremely little power, is generated. For example, at 0.91 Hz and ± 25 degrees, the commercial device produces zero power. However, at 1.1 Hz and ± 25 degrees the commercial device produces $\approx 50 \mu\text{W}$. The plucked piezoelectric device shown in this work could produce $42 \mu\text{W}$ at 1 Hz and ± 30 degrees, which is similar to the commercial device at 1.1 Hz. However, the plucked piezoelectric device does not

have the associated fall off to zero power at lower excitations and continues to provide useful power at much lower excitations as indicated in Table 2. Since, people are not moving their arms very vigorously most of the time, it is believed that the plucked flexible piezoelectric design will produce a higher level of average power. However, a detailed comparison of the average performance of the device reported in this work and the commercial device on human subjects remains to be completed.

3. Conclusions

Strongly {001} oriented PZT 52/48 films ($f = 0.99$) were obtained on both sides of flexible Ni substrates up to a thickness of $5.4 \mu\text{m}$. Well-saturated square-shaped P - E hysteresis loops and a low dielectric constant ($\epsilon_r \approx 450$ at 10 Hz) suggest that the sputtered PZT films have a large fraction of c -domains aligned out-of-plane. This produces a high figure of merit for energy harvesters.

Wrist-worn energy harvesters were fabricated, which used magnetic plucking to achieve frequency up-conversion. For the out-of-plane plucking configuration, six trapezoidal-shaped cantilever beams for a wrist-worn harvester utilize space better and have a more uniform strain compared to a rectangular cantilever beam. To validate the functionality, one trapezoidal piezoelectric beam without a proof mass was tested using a vibration shaker at its resonance frequency ($\approx 250 \text{ Hz}$) and a fixed acceleration level (0.15 G). A power density of $2886 \mu\text{W cm}^{-2} \text{ g}^{-2}$ was obtained at a load resistance of $17 \text{ k}\Omega$ for series connection. Six bimorph trapezoidal cantilever beams were assembled into a wrist-worn energy harvester which generates power from very low frequency linear and rotational motion. The device is capable of generating power from very gentle motions such as a slow arm swing during walking and slow rotation of the wrist by ± 90 degrees. After assembly of the wrist-worn device, of the 12 PZT layers (six bimorph PZT beams), 9 functional PZT layers were obtained. Based on the best unimorph output power, the total RMS output power of the device is demonstrated to be $\approx 90 \mu\text{W}$ from the $\pm 90^\circ$ rotation on-wrist. Furthermore, the wrist-worn device can generate $42 \mu\text{W}$ from a benchtop pseudo-walking motion intended to mimic slow walking, which compares well with the state of the art. The obtained results indicate that these wrist-worn harvesters are able to generate significant power from real-world multidimensional human motion inputs.

4. Experimental Section

Optimization of High-Temperature Sputtering: Optimization of the high-temperature sputtering conditions was undertaken by sputtering PZT onto platinized silicon wafers (Nova Electronic Materials, Flower Mound, TX) with and without a randomly oriented PZT seed layer; the seed layers were prepared by sputtering at room temperature with postdeposition annealing (the deposition conditions are described in Table S1, Supporting Information). A PZT (52/48) ceramic target (manufacturer: Kurt J. Lesker) with 10% excess PbO was used. The growth of $\approx 2 \mu\text{m}$ thick PZT was carried out in an atmosphere of either Ar gas or an Ar/O₂ mixture, at a chamber pressure of 8 mTorr, a power of 90 W for 59 994 s. Figure S3 (Supporting Information) exhibits a schematic of a substrate loaded into the chamber for high-temperature sputtered PZT films. In the sputter system, the substrate set temperature strongly depended on the type of holders (e.g., old and new holder described in detail in Figure S4, Supporting Information) used for this work.

For sputtered PZT films on Ni foil, a custom substrate holder was used because it is suitable to transfer thermal energy efficiently from the heat source (IR lamp) to the substrate, while maintaining a uniform thermal distribution as shown in Figure S9 (Supporting Information). For fabrication of bimorph blanket PZT film on Ni foils by high-temperature sputtering, the Ni substrate required the same preparation steps as those described in reference Yeo et al.,^[33] in order to achieve preferred orientation with limited oxidation. Ni foils were first prepared by polishing, then HfO₂ was deposited as a buffer layer, followed by deposition of (100) textured LaNiO₃ as a template layer (see ref. [31] for details). The parameters used for high-temperature rf-magnetron sputtering (Kurt J. Lesker) including the target composition, chamber pressure, gas composition, power, and temperature are listed in Table S1 (Supporting Information).

Fabrication of Wrist-Worn Harvester: The wrist-worn device utilized a flower petal design with six fixed-free trapezoidal PZT beams (Figure 3). These devices used continuous (001) textured bimorph PZT films on Ni foil (50 μm) prepared by high-temperature sputtering.

As shown in Figure S11 (Supporting Information), the mask layout consists of six individual 1.54 cm² (active area) trapezoidal beams prepared from a 5 × 5 cm² continuous PZT (5.4 μm)/Ni (50 μm)/PZT (5.4 μm) bimorph. The top electrode (red area) was designed to be a little smaller than the actual beam area to avoid extended damage near the edge induced by cutting (with a 150 μm gap). The electrode pads were designed to make the connection over the clamped area where the beams were extended beyond the actual working area for each beam. This gives easy access for wiring with silver paste and Kapton tape. While wire-bonding in principle provides precise contact, it is difficult to apply to a flexible Ni foil, so a manual approach was utilized instead.

Following lift-off processing for the top electrode, both 100 nm thick Pt top electrodes were deposited using dc-magnetron sputtering at room temperature. The electrical properties of both PZT layers were measured with a 400 μm diameter circular electrode placed on an area of the sample where it is not covered by the top trapezoidal electrode as shown in Figure S12b (Supporting Information). After cutting to shape with scissors, two wires for top electrodes and one wire for bottom electrode were connected using silver paste and Kapton tape (see Figure S12c, Supporting Information). The bottom electrode is only essential to pole the PZT layers in opposite directions for series connection during operation. The sample had high yield ($\approx 80\%$) for the >1 cm² electrodes after using the resurrection treatment.^[27,40]

Figure S12d (Supporting Information) shows trapezoidal beams with permanent magnets attached at the end mounted on the hexagonal frame to clamp the beams. The photo was taken after hot poling each of the beams. Based on the calculated magnet configuration, neodymium magnets (2 mm³) were attached to the weighted eccentric rotor by super glue. In order to attach six beams on the hexagonal frame, each beam was flexed by hand to reduce undesirable strong magnet coupling between the beams. Then, the hexagonal frame with the petal-shaped beams was placed on the casing and fixed via six screws at the corners. Two wires connecting the top electrodes of each beam were soldered on to customized PCB

boards attached on the side of case. Figure S12e (Supporting Information) shows an assembled device on a wrist-worn location.

Supporting Information

Supporting Information is available from the Wiley Online Library or from the author.

Acknowledgements

This work was supported by a National Security Science and Engineering faculty fellowship and the Center for Advanced Self-Powered Systems of Integrated Sensors and Technologies (ASSIST) (funding by NSF grant EEC-1160483).

Conflict of Interest

The authors declare no conflict of interest.

Keywords

flexible metal foils, PZT thin films, rf-sputtering, textures, wearable piezoelectric energy harvesters

Received: February 20, 2018

Revised: May 18, 2018

Published online: July 20, 2018

- [1] S.-G. Kim, S. Priya, I. Kanno, *MRS Bull.* **2012**, *37*, 1039.
- [2] X. Ma, A. Wilson, C. D. Rahn, S. Trolier-McKinstry, *J. Vib. Acoust.* **2016**, *138*, 021005.
- [3] For films, given the mixed boundary conditions (the in-plane strain is known, the out-of-plane stress is zero), the materials figure of merit is approximated as: FoM = $(e_{31f})^2/\epsilon_r$; e_{31f} : film transverse piezoelectric coefficient; and ϵ_r : dielectric constant.
- [4] N. Ledermann, P. Murali, J. Baborowski, S. Gentil, K. Mukati, M. Cantoni, A. Seifert, N. Setter, *Sens. Actuators, A* **2003**, *105*, 162.
- [5] T. Fujii, Y. Hishinuma, T. Mita, T. Naono, *Sens. Actuators, A* **2010**, *163*, 220.
- [6] Y. Kokaze, I. Kimura, T. Jimbo, M. Endo, M. Ueda, K. Suu, *ULVAC Tech. Journal* **2007**, *66E*, 13.
- [7] M. Rezaei, J. Luke, D. Rabound, W. Moussa, *Microsyst. Technol.* **2013**, *19*, 1195.
- [8] C. B. Yeager, S. Trolier-McKinstry, *J. Appl. Phys.* **2012**, *112*, 074107.
- [9] F. Calame, P. Murali, *Appl. Phys. Lett.* **2007**, *90*, 2907.
- [10] S. Trolier-McKinstry, F. Griggio, C. Yeager, P. Jousse, D. Zhao, S. S. N. Bharadwaja, T. N. Jackson, S. Jesse, S. V. Kalinin, K. Wasa, *IEEE Trans. Ultrason. Ferroelectr. Freq. Control* **2011**, *58*, 1782.
- [11] M. Lee, C.-Y. Chen, S. Wang, S. N. Cha, Y. J. Park, J. M. Kim, L.-J. Chou, Z. L. Wang, *Adv. Mater.* **2012**, *24*, 1759.
- [12] D. Han, K.-S. Yun, *Microsyst. Technol.* **2015**, *21*, 1669.
- [13] V. Misra, A. Bozkurt, B. Calhoun, T. Jackson, J. S. Jur, J. Lach, B. Lee, J. Muth, O. Oralman, M. Ozturk, S. Trolier-McKinstry, D. Vashae, D. Wentzloff, Y. Zhu, *Proc. IEEE* **2015**, *103*, 665.
- [14] M. Pozzi, M. S. H. Aung, M. Zhu, R. K. Jones, J. Y. Goulermas, *Smart Mater. Struct.* **2012**, *21*, 075023.
- [15] P. Pillatsch, E. M. Yeatman, A. S. Holmes, *J. Phys.: Conf. Ser.* **2013**, *476*, 012010.
- [16] T. Xue, S. Roundy, *Sens. Actuators, A* **2017**, *253*, 101.

- [17] R. Lockhart, P. Janphuang, D. Briand, N. F. De Rooij, *Proc. IEEE Int. Conf. Micro Electro Mech. Syst.* **2014**, 27, 370.
- [18] K. Fan, J. Chang, F. Chao, W. Pedrycz, *Energy Convers. Manage.* **2015**, 96, 430.
- [19] N. A. Shench, J. A. Paradiso, *IEEE Micro* **2001**, 21, 30.
- [20] S. Maiti, S. K. Karan, J. Lee, A. D. Mishra, B. B. Khatua, J. K. Kim, *Nano Energy* **2017**, 42, 282
- [21] S. Lee, S. H. Bae, L. Lin, Y. Yang, C. Park, S. W. Kim, Z. L. Wang, *Adv. Funct. Mater.* **2013**, 23, 2445.
- [22] R. N. Castellano, *J. Vac. Sci. Technol.* **1980**, 17, 629.
- [23] G. Velu, D. Remiens, *Vacuum* **2000**, 56, 199.
- [24] S. B. Krupanidhi, N. Maffei, M. Sayer, K. El-Assal, *J. Appl. Phys.* **1983**, 54, 6601.
- [25] A. Pignolet, R. A. Roy, J. P. Doyle, J. J. Cuomo, *J. Vac. Sci. Technol., A* **1994**, 12, 2840.
- [26] E. Sato, Y. Huang, M. Kosci, A. Bell, N. Setter, *Appl. Phys. Lett.* **1994**, 65, 2678.
- [27] R. H. T. Wilke, R. L. Johnson-Wilke, V. Cotroneo, W. N. Davis, P. B. Reid, D. A. Schwartz, S. Trolrier-McKinstry, *Appl. Opt.* **2013**, 52, 3412.
- [28] P. Murali, *J. Appl. Phys.* **2006**, 100, 51605.
- [29] A. Rajashekhar, A. Fox, S. S. N. Bharadwaja, S. Trolrier-McKinstry, *Appl. Phys. Lett.* **2013**, 103, 032908.
- [30] C. K. Kwok, S. B. Desu, *J. Mater. Res.* **1993**, 8, 339.
- [31] K. Wasa, T. Matsushima, H. Adachi, I. Kanno, H. Kotera, *J. Microelectromech. Syst.* **2012**, 21, 451.
- [32] H. G. Yeo, S. Trolrier-McKinstry, *J. Appl. Phys.* **2014**, 116, 014105.
- [33] H. G. Yeo, X. Ma, C. Rahn, S. Trolrier-McKinstry, *Adv. Funct. Mater.* **2016**, 26, 5940.
- [34] G. R. Fox, S. B. Krupanidhi, K. L. More, L. Allard, *J. Mater. Res.* **1993**, 8, 2191.
- [35] J. A. Voigt, B. A. Tuttle, T. J. Headley, L. Lamppa, *MRS Online Proc. Libr.* **1995**, 361, 395.
- [36] A. H. Carim, B. A. Tuttle, D. H. Doughty, S. L. Martinez, *J. Am. Ceram. Soc.* **1991**, 74, 1455.
- [37] M. M. Samantaray, A. Gurav, E. C. Dickey, C. A. Randall, *J. Am. Ceram. Soc.* **2012**, 95, 257.
- [38] S. Roundy, E. S. Leland, J. Baker, E. Carleton, E. Reilly, E. Lai, B. Otis, J. M. Rabaey, P. K. Wright, V. Sundararajan, *IEEE Pervasive Comput.* **2005**, 4, 28.
- [39] Kinetron, Micro Generator System "26.4," 2014, <http://www.kinetron.eu/wp-content/uploads/2015/01/MGS-26.4.pdf> (accessed: September 2017).
- [40] R. L. Johnson-Wilke, R. H. Wilke, V. Cotroneo, W. N. Davis, P. B. Reid, D. A. Schwartz, S. Trolrier-McKinstry, *Proc. SPIE* **2012**, 8503, 85030A.